

# Rethinking Classifier and Adversarial Attack

Youhuan Yang<sup>1,2</sup>, Lei Sun (✉)<sup>2</sup>, Leyu Dai<sup>2</sup>, Song Guo<sup>2</sup>, Xiuqing Mao<sup>2</sup>, Xiaoqin Wang<sup>2</sup>, Bayi Xu<sup>1,2</sup>

<sup>1</sup> School of Cyber Science and Engineering, Zhengzhou University, Zhengzhou 450000, China

<sup>2</sup> Information Engineering University, Zhengzhou 450001, China

**Abstract** Various defense models have been proposed to resist adversarial attack algorithms, but existing adversarial robustness evaluation methods always overestimate the adversarial robustness of these models (i.e., not approaching the lower bound of robustness). To solve this problem, this paper uses the proposed decouple space method to divide the classifier into two parts: non-linear and linear. Then, this paper defines the representation vector of the original example (and its space, i.e., the representation space) and uses the iterative optimization of Absolute Classification Boundaries Initialization (ACBI) to obtain a better attack starting point. Particularly, this paper applies ACBI to nearly 50 widely-used defense models (including 8 architectures). Experimental results show that ACBI achieves lower robust accuracy in all cases.

**Keywords** adversarial robustness, representation vector, classification boundaries.

## 1 Introduction

With the rapid development of artificial intelligence, various deep learning/machine learning methods [1–5] are widely used in the fields of face recognition, automatic driving, malicious traffic detection, medical image processing, object detection [6] etc. Although deep learning methods have shown powerful performance, research [7] shows that deep neural networks are extremely vulnerable to adversarial attacks. Adversarial attacks make the model output unreasonable predictions by adding slight perturbations that are difficult to distinguish by human eyes to the input of the neural network. Meanwhile, various defense methods have been proposed to resist adversarial attack algorithms. However, these methods perform suboptimally in face of more advanced attack algorithms. Therefore, model robustness evaluation methods are necessary to evaluate the adversarial robustness of various defense algorithms.

The adversarial robustness evaluation method of the trained model specifies the test data set and a certain number of iterations to find its worst performance. Under such task requirements, white-box attack algorithms (assuming that the attacker knows all the information of the model) are widely used to evaluate the adversarial robustness of defense models because of their strong attack performance, e.g., Fast Gradient Sign Method (FGSM) [8], Basic Iterative Method (BIM) [9], Projected Gradient Descent (PGD) [10], Carlini & Wagner (CW) [11], Fast Adaptive Boundary Attack (FAB) [12], etc. Adversarial attacks could be expressed as generating an adversarial perturbation  $\delta$  on a given example pair  $(x, y)$  such that the output of the model  $f$  is  $f(x + \delta) \neq y$ . The adversarial disturbance  $\delta$  is generally generated by multi-step it-

eration, and to enhance the strength of adversarial attacks, many algorithms do not generate adversarial examples from the original example  $x$  ( $x \in [0, 1]^D$ ) as the starting point. Instead, they use the initialization strategy to generate an initial  $\delta_0$  ( $\delta_0 \in [-\epsilon, +\epsilon]^D$ ) and then perform an iterative attack (such as PGD, etc.) on  $x_{st} = x + \delta_0$ , where  $\epsilon$  is an important hyperparameter that restricts the adversarial disturbance to the naked eye, i.e.,  $\epsilon$ -ball constraint (sometimes called box-constraint). Although this random strategy enables the attack algorithm to evaluate the adversarial robustness of the defense model from multiple directions, it is suboptimal because it ignores the relationship between the attack starting point  $x_0$  and model classification boundaries that need adversarial robustness evaluation. Through experiments, it is found that the closer the starting point of the attack algorithm is to the nearest classification boundary of the trained model, the easier it is to generate adversarial examples.

The contributions of this paper are summarized as follows:

- This paper uses proposed decouple space to divide the classifier  $f$  into two sub-models  $f_h$  and  $f_t$ , where  $f_t$  stands for the last layer at the tail of the neural network (fully connected layer, and the number of output neurons is the number of categories), and  $f_h$  stands for all other layers in the head. This paper defines the space between  $f_h$  and  $f_t$  as a representation space (the vector under this space is called the representation vector, which represents an example point in the original space). Using this partitioning method, this paper divides the classifier prediction problem into two problems (a non-linear problem and a linear problem) and gives an expression for the absolute classification boundaries of any classifier.
- This paper proposes a new adversarial perturbation initialization strategy called ACBI based on absolute classification boundaries. ACBI optimizes the distance between the representation vector and the nearest absolute classification boundary by the gradient descent method to obtain a better attack starting point, thereby improving the reliability (approaching the lower bound of robustness) and efficiency (needs fewer iterations to achieve a successful attack) of the existing adversarial robustness evaluation methods.
- This paper evaluates adversarial robustness by using ACBI-based adversarial attack algorithms on more than 50 defense methods. Experiments show that ACBI makes different defense models achieve lower accuracy under different attack algorithms.

## 2 Preliminaries

Many adversarial attack algorithms, e.g., FGSM, BIM, and other algorithms, attack from the original example point. By contrast, PGD, FAB, etc. attack from a random starting point near the original example point each time they restart the attack. This paper selects PGD and FAB attack algorithms for subsequent discussions and experiments because the attack processes and loss functions used by these two algorithms are quite different. Also, other adversarial attack algorithms are more or less similar to PGD and FAB, e.g., FGSM, BIM, CW, the improved versions of PGD, etc. are similar to PGD, and DeepFool [13] and AutoAttack [14] are similar to FAB.

The adversarial attack process of PGD is as follows:

$$x_{adv}^{t+1} = Proj_{(x,\epsilon)}(x_{adv}^t + \alpha sign(\nabla_{x_{adv}^t} \mathcal{L}(f(x_{adv}^t), y))) \quad (1)$$

where,

$$\begin{aligned} x_{adv}^0 &= x_{orig} + \delta_0 \\ x_{orig}, x_{adv}^0 &\in [0, 1]^D \\ \delta_0 &\in [-\epsilon, +\epsilon]^D \end{aligned}$$

In Eq. (1),  $sign$  is the sign function;  $t$  is the  $t$ -th attack iteration number;  $x_{orig}$  denotes the original image;  $\delta_0$  denotes the randomly initialized noise;  $Proj_{(x,\epsilon)}$  clips the input to the  $\epsilon$ -ball of  $x$ ;  $\alpha$  is the step size of a single attack;  $\mathcal{L}$  denotes the loss function.

The process of generating adversarial examples using FAB is as follows:

$$x_{adv}^{t+1} = Proj_C((1 - \beta)(x_{adv}^t + \eta \delta_{adv}^t) + \beta(x_{orig} + \eta \delta_{orig}^t)) \quad (2)$$

where,

$$x_{adv}^0 \leftarrow x_{orig} \text{ or } x_{adv}^0 \leftarrow \text{random sampled s.t. } \|x_{adv}^0 - x_{orig}\|_p = \mu$$

$$\begin{aligned} \delta &= Proj_p(x, \pi_s, C) - x \\ \beta &= \min \frac{\|\delta_{adv}^t\|_p}{\|\delta_{adv}^t\|_p + \|\delta_{orig}^t\|_p}, \beta_{max} \in [0, 1] \end{aligned}$$

In Eq.(2),  $\beta$  is a balance parameter using historical information;  $\eta$  is a hyperparameter that controls the size of the perturbations;  $\mu$  is a parameter that limits the initial size of the starting point;  $\|\bullet\|_p$  denotes  $L - p$  norm;  $Proj_C$  is the projection onto the box (or box constraints), and it can be realized by clipping; operation  $Proj_p(x, \pi_s, C)$  will projects  $x$  onto  $\pi_s$  and then clips value to the box-constraint;  $\pi_s$  represents the approximate hyperplane at the example point  $x_{adv}^t$ . For details, please refer to [12].

From the calculation process of PGD and FAB, it can be found that  $x_{adv}^0$  is randomly selected from the vicinity of  $x_{orig}$  as the starting point to attack (of course,  $x_{adv}^0$  needs to meet the box-constraint). Obviously, these starting points are sub-optimal. To handle this problem, this paper proposes an ACBI strategy, and the implementation details will be presented in the next section.

## 3 ACBI: Absolute Classification Boundaries Initialization

### 3.1 Revisit the classifier

**Traditional perspective:** generally, a classifier is composed of multiple network layers (convolution, pooling, fully connected, non-linear activation functions, etc.). The non-linear activation function (such as ReLu, Sigmoid, etc.) is the key to the non-linearity of one classifier.

$$z = f(x) = f_{\dots}(f_2(f_1(x))) \quad (3)$$

where  $f_i$  is a single network layer in the classifier. Many researchers treat the classifier as  $f$  (obviously  $f$  is non-linear) and discuss various problems of the classifier as a whole. In this case, many linear solutions cannot be directly applied to  $f$ . Therefore, studies [8, 12, 15] assume that  $f$  can be approximately regarded as a linear expression. However, these studies are all suboptimal.

**New perspective:** first of all, this paper ignores the softmax (or sigmoid) function during classifier inference. This is because these functions are often used to normalize the output logits of the model as the predicted probability, which is strictly monotonically increasing. Also, the presence or absence of these functions will not affect the Absolute Classification Boundaries of the classifier (this will be explained in the next section). Therefore, this paper does not discuss the case where the final output of the classifier passes through activation functions such as softmax without any special instructions.

This paper splits the classifier into two parts,  $f_h$  and  $f_i$ , where  $f_i$  represents the last layer of the classifier (a fully connected layer, the output dimension is  $K$ , i.e.,  $K$  categories for a classification task), and  $f_h$  represents all other network layers of the classifier (except the last layer). This paper refers to this as decouple space. Given an example pair  $(x, y)$  ( $x$  is the model input and  $y$  is the one-hot encoded example label), then the output of the classifier  $z$  ( $z \in \mathbb{R}^K$ ,  $z_i$  is the score given by the classifier on the  $i$ -th class) can be expressed as:

$$z = f(x) = f_i(v) = wv + b \quad (4)$$

where,

$$v = f_h(x) \quad (5)$$

This paper regards  $v$  as a representation vector of example point  $x$  in  $N$ -dimensional space ( $v \in \mathbb{R}^N$ ,  $w \in \mathbb{R}^{(K,N)}$ ,  $b \in \mathbb{R}^K$ ). It is worth noting that multiple example points in the  $N$ -dimensional space may correspond to a representation vector. It is difficult to reverse map from  $v$  back to  $x$  due to the existence of irreversible operations such as ReLu [16], MaxPooling etc.

$$x \xrightarrow{f_h} v \xrightarrow{f_i} z \quad (6)$$

Thus, this paper divides the non-linear  $f$  into two parts following Eq. (6) while maintaining the non-linear  $f_h$  and linear  $f_i$ . All linear analysis methods and solutions can be applied when only the linear classifier  $f_i$  is considered and  $f_h$  is ignored.

### 3.2 Decision boundary

**Fuzzy Boundary:** in the traditional view, the notion of boundaries is ambiguous because the classifier is highly non-linear. Many researchers choose to use the input  $x$  and output  $z$  to approximately fit some curves [17–19] and regard these curves as the classification boundaries of the classifier. However, this approach has two disadvantages: 1) the quality of the curve fitting and the degree of deviation from the true classification boundary depend on the prediction accuracy of the classifier and its generalization. 2) the exact expression of the classification boundaries cannot be given, so these boundaries cannot be used to solve some problems. In view of these disadvantages, some researchers adopt a suboptimal solution, treat the non-linear classifier as a linear map approximately [8, 12], and apply some linear analysis to solve problems. Of course, these methods work well when the size of the classifier is small (e.g. MLP or Small CNN), but the approximate linearity is poor for the current mainstream large or huge classifiers (e.g. ResNet-18 [2] or WRN34-10 [5]).

**Absolute Boundary:** this paper proposes Absolute Boundaries based on the decouple space, which only uses  $f_i$  to calculate the expression of absolute boundaries (different from fuzzy boundaries, the independent variable of absolute boundaries expression is the representation vector  $v$  rather than the original example  $x$ ). The calculation of these expressions is introduced as follows.

Assuming that example  $x$  belongs to the  $i$ -th class, the requirements for making the classifier's prediction result correct are as follows:

$$i = \operatorname{argmax} z \quad (7)$$

and

$$\forall j \in [0, K), j \neq i$$

$$\begin{aligned} F_{(i,j)}(v) &= z_i - z_j > 0 \\ &= w_i v + b_i - (w_j v + b_j) > 0 \\ &= (w_i - w_j)v + (b_i - b_j) > 0 \\ &= w_{(i,j)}v + b_{(i,j)} > 0 \end{aligned} \quad (8)$$

It can be seen that non-linear normalization functions such as softmax will not affect the results of Eq. (7) and Eq. (8), so this paper ignores these non-linear factors. In Eq. (8),  $w_{(i,j)}$  is the difference vector of the  $i$ -th and  $j$ -th dimension vectors of the weight parameter  $w$ . The above formula indicates that a set of inequality equations actually determines which category the classifier predicts. There are  $K - 1$  inequality equations in total, and the prediction score  $z_i$  of the  $i$ -th dimension needs to be larger than the prediction scores  $z_j$  of all other categories. The same is true for predicting other categories.

For the convenience of discussion, this paper ignores the case where the values of the two dimensions in the prediction  $z$  are the same and both are the largest (corresponding to  $F_{(i,j)}(v) = 0$  in Eq. (8)), this situation is almost impossible and is not helpful for our analysis. Thus,  $F_{(i,j)}(v) > 0$  is a necessary and insufficient condition for the classifier to predict the  $i$ -th class (of course,  $F_{(i,j)}(v) < 0$  is a necessary and insufficient condition for the classifier to predict the  $j$ -th class). This paper defines  $F_{(i,j)}(v) = 0$  as the classification decision equation of the classifier for the  $i$ -th class and the  $j$ -th class. According to the above discussion, this paper gives the necessary and sufficient conditions for the classifier to predict the  $i$ -th class as (i.e., the equivalent expression of Eq. (7)):

$$F_i(v) > 0 \leftarrow \bigcap_{i,j \in [0,K), i \neq j} F_{(i,j)}(v) > 0 \quad (9)$$

The set of equations composed of classification decision equations between all categories ( $i \neq j$ ) is:

$$\begin{aligned} F &= \{F_{(0,1)}(v) = 0, \dots, F_{(i,j)}(v) = 0, \dots, F_{(K-2,K-1)}(v) = 0\} \\ &= \{w_{(0,1)}v + b_{(0,1)} = 0, \dots, \\ &\quad w_{(i,j)}v + b_{(i,j)} = 0, \dots, \\ &\quad w_{(K-2,K-1)}v + b_{(K-2,K-1)} = 0\} \\ &= \{\mathcal{W}v + \mathcal{B} = 0\} \end{aligned} \quad (10)$$

It is worth noting that  $F_{(i,j)}(v) = 0 \Leftrightarrow F_{(j,i)}(v) = 0$ ,  $F_{(i,j)}(v) > 0 \Leftrightarrow F_{(j,i)}(v) < 0$ . Therefore,  $F$  contains a total of  $C_K^2$  (i.e.,  $K(K-1)/2$ ) classification decision equations

(a total of  $K - 1$  ones related to the  $i$ -th class). So, for any  $v \in \mathbb{R}^N$ ,  $F$  divides  $\mathbb{R}^N$  into  $K$  subspaces (corresponding to  $K$  categories), and there is no intersection between any two spaces, that is:

$$\begin{aligned} & \forall v \in \mathbb{R}^N \\ & \mathbb{R}^N = \bigcup_{k=0}^{K-1} S_k (S_i \cap S_j = \emptyset, i, j \in [0, K] \ i \neq j) \\ & \text{s.t. } v \in S_k (\text{or } F_k(v) > 0) \end{aligned} \quad (11)$$

The above definitions of the classification decision equations and the division of the representation vector spaces ( $v \in \mathbb{R}^N$ ) are curial. All problems in this space are linear, and all the following discussions are conducted in this representation vector space.

### 3.3 How adversarial attacks work

Although various deep learning methods show strong performance, Szegedy et al. [7] found that adding a slight perturbation that is difficult to distinguish with the naked eye to the input image can fool the classifier and make it obtain wrong prediction results. For any example  $x$  (assuming it belongs to class  $y$ ), the adversarial attack can be expressed as follows:

$$\begin{aligned} & y \neq \operatorname{argmax} f(x + \delta) \\ & \text{s.t. } x + \delta \in [0, 1]^D, \|\delta\|_p \leq \epsilon \end{aligned} \quad (12)$$

where  $\delta$  denotes adversarial perturbation, and  $\|\cdot\|_p$  denotes the  $L - p$  distance used to limit the size of the adversarial perturbation. This paper uses the commonly used  $L - \infty$  attack method ( $\|\delta\|_\infty \leq \epsilon$ ) without special instructions.

Under the operation of the decouple space, adversarial attacks can be expressed in the representation space as follows:

$$\begin{aligned} & x + \delta \xrightarrow{f_h} v + \Delta v \\ & F_k(v + \Delta v) > 0 (\text{or } v + \Delta v \in S_k) \text{ and } k \neq y, k \in [0, K] \end{aligned} \quad (13)$$

In this way, adversarial attacks actually add a slight perturbation  $\delta$  to the original input  $x$  so that there is an increment  $\Delta v$  in the representation space, and  $\Delta v$  makes  $v$  located in the non-label domain (i.e.,  $v + \Delta v \notin S_y$ ). Meanwhile, when  $k$  in Eq. (13) is designated manually, it is a target attack; otherwise, it is a non-target attack.

Fig. 1 shows the attack scenario of the adversarial attack in the representation space. The attacked model is a small convolutional neural network (two convolutional layers followed by BatchNormalization [20], ReLu and MaxPooling layers, and the size of the output channels are 16 and 32, respectively; then, followed by two fully connected layers with

output units of  $N$  and  $K$  respectively). The model is trained with the MNIST data. In particular, the experiment shown in Fig. 1 only selected four categories of pictures (number 0, 1, 2, and 3) in partial MNIST, and the representation space is reduced to 2 dimensions, mainly to make the representation space displayable ( $N = 2$ ) and reduce the clutter of elements in the space ( $K = 4$ ).

Fig. 1 shows the attack effect of BIM-10 at each step on partial MNIST, where each line represents the absolute classification decision boundary between any two categories obtained by Eq. (8). The color of all points represents the true category to which they belong, and the shape of the points represents a different type of example.  $\square$  and  $\bullet$  represent the original example points, and  $\times$  and  $\star$  represent the adversarial examples generated by BIM (one-to-one correspondence with the original example points). If the generated adversarial sample is correctly predicted by the classifier, the adversarial example is represented by  $\star$  (the corresponding original example point is represented by  $\bullet$ ); otherwise, the adversarial example is represented by  $\times$  (the corresponding original example point is represented by  $\square$ ). Note that Fig. 1 only shows the correctly predicted original example points and their corresponding adversarial example points. It can be observed that the iterative attack process of iterative adversarial attack algorithms (BIM, PGD, etc.) gradually migrates (each sub-figure in Fig. 1) the original examples from the region  $S_y$  to  $S_k$  ( $k \neq y$ ).

### 3.4 Apply ACBI to adversarial robustness evaluation algorithm

As introduced in the previous introduction, the entire adversarial attack process is to add a limited increment  $\Delta v$  to the representation vector  $v$  so that  $v + \Delta v$  gradually approaches the classification decision boundary until it crosses the boundary (the attack is successful). It can be seen from Fig. 1 that the example points closer to the classification decision boundary are more vulnerable to attack. Therefore, this paper proposes the ABCI method. Different from the original random initialization (RI), ACBI uses the geometric information of the representation space to purposefully initialize the starting point of the attack and improves the effectiveness of the attack algorithm. The difference between ACBI and RI is shown in Fig. 2.

In Fig. 2, the left side shows the original input space, and the right side shows the representation space of the original space example points mapped by  $f_h$ . The blue points in the representation space are generated by random initialization,



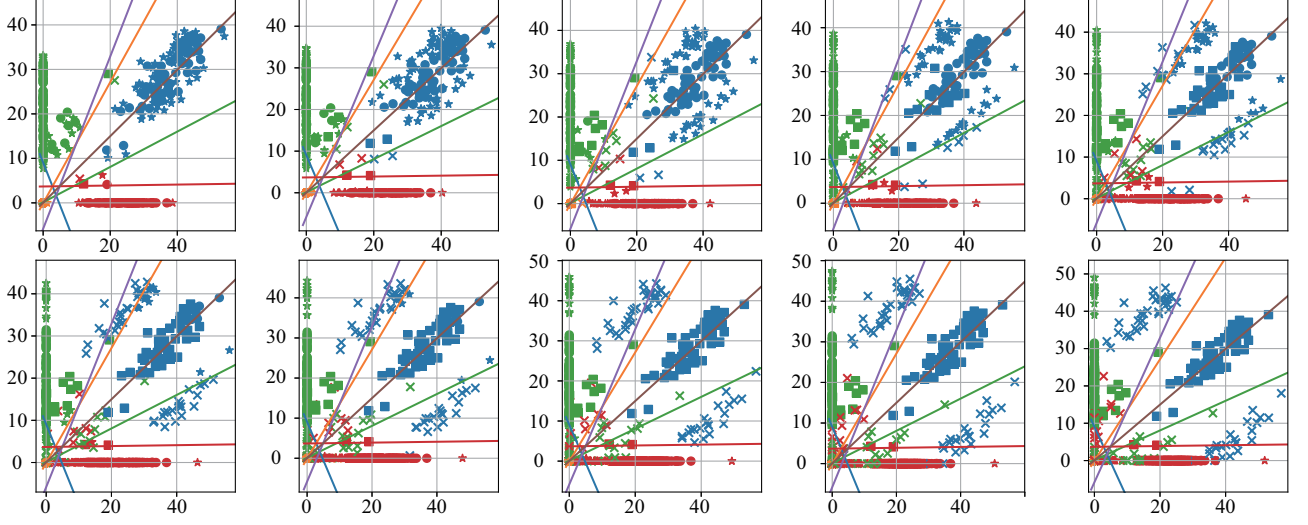


Fig. 1: Effects of BIM on representation vectors on partial MNIST

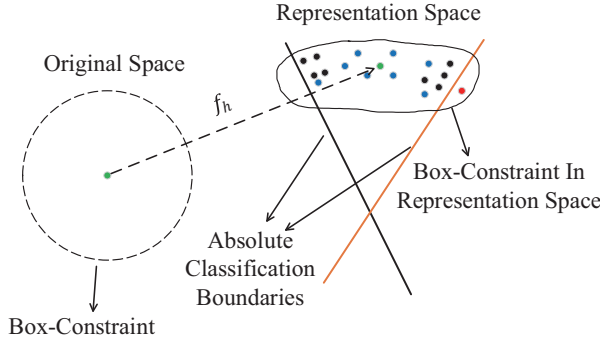


Fig. 2: Comparison of ACBI and RI

the black points are generated using the ACBI method, and the two lines represent the absolute classification decision boundaries of the model. It can be seen that the initial points generated by ACBI are better than those generated by the RI method. They are not distributed around the representation vector but near the absolute classification boundaries, which will make it easier for the adversarial attack algorithm to use these starting points to attack faster and more efficiently.

It is theoretically possible to obtain an adversarial example (represented as a red dot in Fig. 2) that is wrongly predicted by the classifier through the absolute classification boundary, but this is very difficult in practice. The mapping from the original space to the representation space only needs to use  $f_h$ . However, due to the existence of irreversible mapping

functions such as ReLu and MaxPooling, the reverse mapping  $f_h^{-1}$  from the representation space to the original space cannot be described. Therefore, this paper uses ACBI to perform multiple iterations to obtain an initial point closer to the absolute classification boundary and then uses the original attack algorithm for iterative attacks.

First, this paper defines the distance from the representation vector  $v$  (assuming its true label belongs to the  $y$ -th class) to the absolute classification boundary associated with the  $k$ -th class ( $k \in [0, K], k \neq y$ ) as:

$$\mathbb{D}(v, y, k) = \frac{F_{(y,k)}(v)}{\sqrt{\sum w_{(y,k)}^2}} \quad (14)$$

The difference between Eq. (14) and the traditional geometric distance definition is that it has a direction (i.e.,  $\mathbb{D}$  may be a negative value), and the positive or negative of  $\mathbb{D}(v, y, k)$  is positive or negative depending on which side of the line  $F_{(y,k)} = 0$  the representation vector  $v$  falls on. If  $\mathbb{D}(v, y, k) < 0$ , it is indicated that  $v$  falls into the  $S_y$  area, and the smaller the value, the farther it is from the area  $S_y$  where the label is located.

In view of the above discussion, this paper gives the calculation process of ACBI. In each restart, a starting point is randomly selected to ensure the diversity of each restart:

$$x_{st} = x + \delta_0 \quad (15)$$

where  $\delta_0 \in U(-\epsilon, +\epsilon)^D$ . Then,  $x_{st}$  is used as the iteration starting point to initialize using Eq. (14) and the gradient descent method to obtain a start point that closer to the clas-

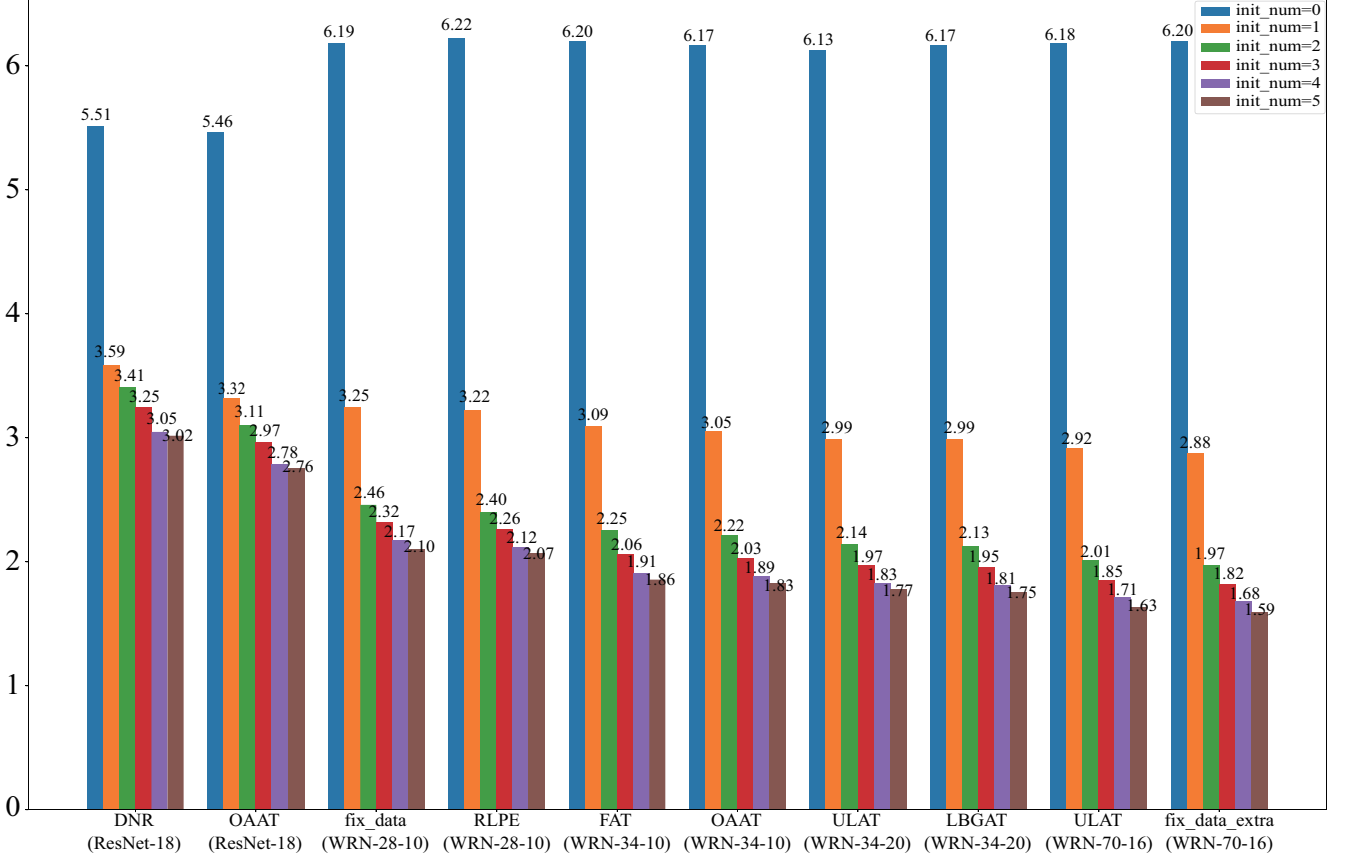


**Fig. 3: Iteration number until attack success**

sification decision boundary:

$$x_{init}^{t+1} = P_{(x,\epsilon)}(x_{init}^t - \eta_{init} \text{sign}(\nabla_{x_{init}^t} \mathbb{D}(v_{init}^t, y, m))) \quad (16)$$

where,

$$\begin{aligned} x_{init}^0 &= x_{st} \\ v_{init}^t &= f_h(x_{init}^t) \\ m &= \underset{n \neq y}{\operatorname{argmin}} \mathbb{D}(v_{init}^t, y, n) \end{aligned}$$

In Eq. (16),  $\eta_{init}$  is the step size in the iterative process, and function  $P_{(x,\epsilon)}(\bullet)$  clips the input (the starting point obtained by the  $t$ -th iteration) to the  $\epsilon$ -ball of  $x$ . The representation vector will quickly reach its nearest classification decision boundary through multiple initialization iterations.

To demonstrate the effectiveness of ACBI, this paper uses PGD-4-25 (4 restarts, 25 iterations for each restart) with the ACBI method for adversarial robustness evaluation on 10 defense models (including 5 network architectures, namely ResNet-18, WRN-28-10, WRN-34-10, WRN-34-20, WRN-70-16, and 7 defense methods, namely DNR, OAAT, Fixing Data, RLPE, FAT, ULAT, LBGAT). The results are shown in Fig. 3.

The experiments in Fig. (3) use ACBI with 0 to 5 initialization iterations (when the number of ACBI initialization is 0, it is the default version of PGD) on each defense model for attack evaluation. Each bar counts the number of attacks required for ACBI-PGD attacks to succeed under different initialization iterations (mean of iteration numbers for a successful attack in 1000 randomly selected examples from the CIFAR-10 test set). It can be found that the more times the ACBI is initialized, the fewer iterations are required for the attack to succeed (i.e., the better attack starting point obtained by ACBI). That is, when the number of attack iterations is fixed, the performance of the attack algorithm using the ACBI method will be better (approaching the lower bound of robustness).

Algorithm 1 shows how to apply ACBI to existing iterative attack algorithms. Obviously, ACBI does not depend on existing attack algorithms and is parameter-free (do not need to carefully adjust parameters). The specific performance of ACBI will be shown in the experimental section.

---

**Algorithm 1:** Improve Adversarial Attack Using ACBI.

---

**Input:** Example pair  $(x, y)$ , norm bound  $\epsilon$ , the number of restarts  $R$ , the number of iterations for ACBI  $N_{init}$ , the step size for initialization iteration  $\eta_{init}$ , the number of the original attack iterations in each restart  $N_{attack}$ .

**Output:** Adversarial example  $x_{adv}^{t+1}$ .

```
1 for  $r = 0$  to  $R$  do
2   Using Eq.(15) to obtain the random start point  $x_{st}^0$ 
3   for  $t = 0$  to  $N_{init}$  do
4     Using Eq.(16) to obtain  $x_{init}^{t+1}$ 
5   end
6   for  $t = 0$  to  $N_{attack}$  do
7     Using original attack algorithm in each iteration to obtain  $x_{adv}^{t+1}$ 
8   end
9 end
```

---

## 4 Experiment

This paper conducts comprehensive experiments on two datasets, CIFAR-10 and CIFAR-100, to verify the effectiveness of the proposed method. Two adversarial robustness evaluation methods, PGD and FAB, are used for ACBI testing. The main reason is that the loss functions and iterative process involved in the two attack algorithms are quite different, i.e., these are two completely different types of attack algorithms. There are 8 different network structures, and nearly 50  $L - \infty$  defense algorithms are used for adversarial robustness evaluation. Most of the algorithms are selected from recent top conferences, e.g., ICML, NeurIPS, ICLR, ICCV, and CVPR. Experiments show that the adversarial examples generated by the attack algorithm using the ACBI method can make the classifier obtain lower accuracy, indicating that using ACBI can improve the efficiency of the adversarial robustness evaluation method.

This paper uses the original PGD and FAB without the ACBI method as the baseline. The restart number of all attack algorithms is set to 4, and the number of attack iterations is set to 25. For a fair comparison, this paper regards the number of initialization iterations as part of the number of attack iterations, i.e.,  $N_{init} + N_{attack} = 25$ . The hyperparameter  $\eta_{init}$  is set to  $\epsilon$ , and there is no other careful tuning. The experimental results are presented in Table 1 (CIFAR-10) and Table 2 (CIFAR-100).

Table 1 shows the performance of ACBI on PGD-4-25 and FAB-4-25. The first column shows the network architecture and the method name of the defense model (the one marked with  $\ddagger$  is  $\epsilon = 0.031$ , and the one marked with  $\dagger$  is an additional unlabeled dataset used for training); the second column shows the original test example accuracy (Clean).

PGD\* denotes PGD using ACBI strategy with  $N_{init} = 5$  and  $N_{attack} = 20$ ; FAB\* denotes the FAB using ACBI strategy with  $N_{init} = 1$  and  $N_{attack} = 24$ .  $\epsilon$  in the attack process is set to 8.0/255, and the  $\eta_{init}$  in ACBI is equal to  $\epsilon$ . In the experiment, 1000 examples were randomly selected for testing on CIFAR-10. The experimental results show that ACBI obtains different degrees of improvement on PGD and FAB. The smaller the number of model parameters, the better the ACBI performance (e.g., ResNet-18 and WRN-28-10). One of the main reasons for this phenomenon is that the larger the number of parameters (i.e., the more complex  $f_h$ , the stronger the non-linearity of  $f_h$ ), the more difficult it is to optimize the distance from the starting point to the absolute classification decision boundary using Eq. (16). This is reflected in Table 2.

In addition, the improvement brought by ACBI to FAB is significantly smaller than that of PGD, which is related to the attack principle of FAB. FAB regards the classifier as an approximately linear function. It uses the first-order Taylor expansion at the example point  $x$  (true label is  $y$ ) to approximate the decision plane  $\pi_s$  closest to  $x$ . Then, it uses  $Proj_p(x_{adv}^{(i)}, \pi_s, y)$  operation to project the adversarial example  $x_{adv}^{(i)}$  of the  $i$ -th iteration onto the hyperplane and then clips to  $[0, 1]^D$ . Therefore, the classification decision boundary of the model is used in the FAB attack. Although it is approximately estimated (fuzzy), it can still reflect the classification boundary information to a certain extent, so the improvement of ACBI on FAB is lower than that of PGD.

In this paper, the adversarial robustness evaluation performance of ACBI to PGD and FAB on CIFAR-100 is presented in Table 2. The settings of various parameters are consistent with CIFAR-10. The experimental results show that ACBI obtains different degrees of improvement for different types of attack algorithms on more complex data sets.

**Table 1: The performance of ACBI on CIFAR-10**

CIFAR-10 Defense Model		Clean	PGD	PGD*	FAB	FAB*
ResNet-18	Adv_regular [21]	90.58%	74.09%	61.48%(-12.61%)	21.61%	17.53%(-4.08%)
	FBTF [22]	87.85%	60.93%	55.25%(-5.68%)	34.15%	32.34%(-1.81%)
	CNL [23]‡	85.45%	66.90%	51.01%(-15.89%)	36.98%	35.43%(-1.55%)
	Understanding FAST [24]	84.38%	62.57%	51.00%(-11.57%)	39.10%	38.11%(-0.99%)
	Proxy [25]	84.54%	62.02%	53.03%(-8.99%)	42.54%	41.87%(-0.67%)
	DNR [26]	85.04%	59.37%	52.16%(-7.21%)	42.72%	42.27%(-0.45%)
	OAAT [27]	84.34%	58.99%	52.93%(-6.06%)	43.95%	43.62%(-0.33%)
WRN-28-4	mma [28]	86.75%	61.07%	60.29%(-0.78%)	57.60%	57.52%(-0.08%)
ResNet-50	robustness [29]	86.78%	60.84%	60.11%(-0.73%)	57.57%	57.50%(-0.07%)
WRN-28-10	MART [30]†	84.67%	59.54%	54.34%(-5.2%)	45.82%	45.55%(-0.27%)
	Feature_Scatter [31]	85.26%	60.79%	55.93%(-4.86%)	48.03%	47.76%(-0.27%)
	Adv_inter [32]	85.74%	62.01%	57.57%(-4.44%)	50.22%	49.92%(-0.3%)
	awp [33]†	85.90%	62.29%	58.30%(-3.99%)	51.22%	50.95%(-0.27%)
	geometry [17]†‡	86.20%	62.75%	59.17%(-3.58%)	51.95%	51.70%(-0.25%)
	hydra [34]†	86.40%	62.66%	59.42%(-3.24%)	52.87%	52.65%(-0.22%)
	Pre-train [35]	86.41%	62.45%	59.53%(-2.92%)	53.01%	52.82%(-0.19%)
	rst [36]†	86.58%	62.56%	59.89%(-2.67%)	53.46%	53.29%(-0.17%)
	ULAT [37]†	86.76%	62.83%	60.37%(-2.46%)	54.18%	54.02%(-0.16%)
	Fix_data [38]	86.84%	62.93%	60.64%(-2.29%)	54.56%	54.40%(-0.16%)
WRN-34-10	RLPE [39]†	86.98%	62.94%	60.82%(-2.12%)	54.92%	54.76%(-0.16%)
	TRADES [19]‡	86.87%	62.59%	60.61%(-1.98%)	54.83%	54.67%(-0.16%)
	awp [33]	86.82%	62.43%	60.57%(-1.86%)	55.10%	54.98%(-0.12%)
	Proxy_dist [25]†	86.80%	62.50%	60.76%(-1.74%)	55.25%	55.19%(-0.06%)
	Self_adaptive [40]‡	86.65%	62.29%	60.64%(-1.65%)	55.19%	55.12%(-0.07%)
	sensible [41]	86.81%	62.24%	60.70%(-1.54%)	55.14%	55.01%(-0.13%)
	yopo [42]	86.85%	61.58%	60.15%(-1.43%)	54.78%	54.70%(-0.08%)
	IAR/SAT [43]	86.88%	61.30%	59.95%(-1.35%)	54.64%	54.60%(-0.04%)
	LBGAT [44]‡	86.94%	61.05%	59.78%(-1.27%)	54.71%	54.57%(-0.14%)
	FAT [45]	86.85%	60.91%	59.72%(-1.19%)	54.76%	54.64%(-0.12%)
WRN-34-15	OAAT [27]	86.76%	61.03%	59.90%(-1.13%)	54.98%	54.87%(-0.11%)
	RLPE [39]†	86.76%	60.94%	60.23%(-0.71%)	57.68%	57.61%(-0.07%)
WRN-34-20	Hyper-embe [46]	86.68%	61.07%	59.97%(-1.1%)	55.04%	54.94%(-0.10%)
	Overfit [47]	86.64%	60.99%	59.97%(-1.02%)	55.03%	54.94%(-0.09%)
	ULAT [37]	86.59%	61.00%	60.02%(-0.98%)	55.14%	55.05%(-0.09%)
	LBGAT [44]‡	86.63%	60.88%	59.96%(-0.92%)	55.17%	55.05%(-0.12%)
WRN-70-16	ULAT [37]	86.74%	61.12%	60.30%(-0.82%)	56.94%	56.85%(-0.09%)
	ULAT [37]†	86.78%	61.15%	60.28%(-0.87%)	56.50%	56.40%(-0.10%)
	Fix_data [38]	86.79%	61.30%	60.52%(-0.78%)	57.70%	57.62%(-0.08%)

**Table 2: The performance of ACBI on CIFAR-100**

CIFAR-100 Defense Model		Clean	PGD	PGD*	FAB	FAB*
ResNet-18	overfit [47]	51.76%	18.39%	17.71%(-0.68%)	21.87%	19.53%(-2.34%)
	OAAT [27]	57.09%	25.20%	22.53%(-2.67%)	23.43%	22.65%(-0.78%)
WRN-28-10	Pre-train [35]	58.36%	28.35%	25.50%(-2.85%)	26.04%	25.26%(-0.78%)
	Fix-data [38]	59.62%	30.24%	27.58%(-2.66%)	27.14%	26.95%(-0.19%)
WRN-34-10	awp [33]	59.74%	30.66%	27.77%(-2.89%)	26.25%	26.09%(-0.16%)
	IAR/SAT [43]	59.93%	30.01%	27.36%(-2.65%)	25.26%	25.13%(-0.13%)
	LBGAT [44]‡	59.78%	30.75%	28.01%(-2.74%)	26.56%	26.45%(-0.11%)
	OAAT [27]	60.63%	31.60%	28.76%(-2.84%)	27.24%	27.14%(-0.10%)
WRN-34-20	LBGAT [44]‡	60.97%	32.07%	29.09%(-2.98%)	27.77%	27.69%(-0.08%)
WRN-70-16	ULAT [37]	60.72%	32.71%	29.66%(-3.05%)	28.36%	28.30%(-0.06%)
	ULAT [37]†	62.17%	34.14%	31.43%(-2.71%)	31.25%	31.20%(-0.05%)
	Fix-data [38]	62.05%	34.31%	31.81%(-2.50%)	30.95%	30.91%(-0.04%)



All experiments in this paper did not deliberately adjust the parameters, and the experimental results are the average of five groups of repeated experiments. ACBI can be integrated as a module to other attack algorithms, e.g., BIM, CW, etc. Importantly, ACBI and other strategies that improve the reliability of robustness evaluation methods are highly loosely coupled, and they can be used simultaneously in one attack algorithm.

## 5 Conclusion

This paper first proposes the decouple space method to divide the classifier  $f$  into two parts, the non-linear mapping  $f_h$  and the linear mapping  $f_l$ . The original example can obtain its representation vector  $v$  on the  $R^N$  space (referred to as the representation space in this paper) through the mapping of  $f_h$ , and then all linear problem-solving methods can be applied to  $v$ . Then, from the perspective of decouple space, this paper uses  $f$  to define the absolute classification decision boundaries. Unlike the fuzzy boundaries, given any classifier, this paper can obtain the expressions of the absolute classification decision boundaries on  $R^N$ . Next, ACBI is adopted to make the representation vector as close as possible to the nearest classification decision boundary through iterative optimization, thus obtaining a better attack starting point. Finally, the experimental results on more than 50 defense models show that the adversarial robustness evaluation method using ACBI is more reliable than the original ones.

## References

- Cheng, Y., et al., A convolutional neural network based degradation indicator construction and health prognosis using bidirectional long short-term memory network for rolling bearings. *Advanced Engineering Informatics*, 2021. 48: p. 101247.
- He, K., et al. Deep residual learning for image recognition. in *Proceedings of the IEEE conference on computer vision and pattern recognition*. 2016.
- Huang, G., et al. Densely connected convolutional networks. in *Proceedings of the IEEE conference on computer vision and pattern recognition*. 2017.
- Szegedy, C., et al. Rethinking the inception architecture for computer vision. in *Proceedings of the IEEE conference on computer vision and pattern recognition*. 2016.
- Zagoruyko, S. and N. Komodakis, Wide residual networks. *arXiv preprint arXiv:1605.07146*, 2016.
- Chiu, M.-C., H.-Y. Tsai, and J.-E. Chiu, A novel directional object detection method for piled objects using a hybrid region-based convolutional neural network. *Advanced Engineering Informatics*, 2022. 51: p. 101448.
- Szegedy, C., et al., Intriguing properties of neural networks. *arXiv preprint arXiv:1312.6199*, 2013.
- Goodfellow, I.J., J. Shlens, and C. Szegedy, Explaining and harnessing adversarial examples. *arXiv preprint arXiv:1412.6572*, 2014.
- Kurakin, A., I. Goodfellow, and S. Bengio, Adversarial examples in the physical world. 2016.
- Madry, A., et al., Towards deep learning models resistant to adversarial attacks. *arXiv preprint arXiv:1706.06083*, 2017.
- Carlini, N. and D. Wagner, Towards Evaluating the Robustness of Neural Networks, in *2017 IEEE Symposium on Security and Privacy (SP)*. 2017. p. 39-57.
- Croce, F. and M. Hein. Minimally distorted adversarial examples with a fast adaptive boundary attack. in *International Conference on Machine Learning*. 2020. PMLR.
- Moosavi-Dezfooli, S.-M., A. Fawzi, and P. Frossard. Deepfool: a simple and accurate method to fool deep neural networks. in *Proceedings of the IEEE conference on computer vision and pattern recognition*. 2016.
- Croce, F. and M. Hein. Reliable evaluation of adversarial robustness with an ensemble of diverse parameter-free attacks. in *International conference on machine learning*. 2020. PMLR.
- Liu, Y., et al., Practical evaluation of adversarial robustness via adaptive auto attack. *arXiv preprint arXiv:2203.05154*, 2022.
- Krizhevsky, A., I. Sutskever, and G.E. Hinton, Imagenet classification with deep convolutional neural networks. *Advances in neural information processing systems*, 2012. 25.
- Zhang, J., et al., Geometry-aware instance-reweighted adversarial training. *arXiv preprint arXiv:2010.01736*, 2020.
- Gao, R., et al., Maximum mean discrepancy is aware of adversarial attacks. *arXiv preprint arXiv:2010.11415*, 2020.
- Zhang, H., et al. Theoretically principled trade-off between robustness and accuracy. in *International Conference on Machine Learning*. 2019. PMLR.
- Ioffe, S. and C. Szegedy. Batch normalization: Accelerating deep network training by reducing internal covariate shift. in *International conference on machine learning*. 2015. PMLR.
- Jin, C. and M. Rinard, Manifold regularization for adversarial robustness. *arXiv preprint arXiv:2003.04286*, 2020. 1.
- Wong, E., L. Rice, and J.Z. Kolter, Fast is better than free: Revisiting adversarial training. *arXiv preprint arXiv:2001.03994*, 2020.
- Atzmon, M., et al., Controlling neural level sets. *Advances in Neural Information Processing Systems*, 2019. 32.
- Andriushchenko, M. and N. Flammarion, Understanding and improving fast adversarial training. *Advances in Neural Information Processing Systems*, 2020. 33: p. 16048-16059.
- Sehwag, V., et al., Improving adversarial robustness using proxy distributions. *arXiv preprint arXiv:2104.09425*, 2021.
- Kundu, S., et al. DNR: A tunable robust pruning framework through dynamic network rewiring of DNNs. in *Proceedings of the 26th Asia and South Pacific Design Automation Conference*. 2021.

27. Addepalli, S., et al., Towards Achieving Adversarial Robustness Beyond Perceptual Limits. 2021.
28. Ding, G.W., et al., Mma training: Direct input space margin maximization through adversarial training. arXiv preprint arXiv:1812.02637, 2018.
29. Engstrom, L., et al., Robustness (python library). 2019.
30. Wang, Y., et al. Improving adversarial robustness requires revisiting misclassified examples. in International Conference on Learning Representations. 2019.
31. Zhang, H. and J. Wang, Defense against adversarial attacks using feature scattering-based adversarial training. Advances in Neural Information Processing Systems, 2019. 32.
32. Zhang, H. and W. Xu, Adversarial interpolation training: A simple approach for improving model robustness. 2019.
33. Wu, D., S.-T. Xia, and Y. Wang, Adversarial weight perturbation helps robust generalization. Advances in Neural Information Processing Systems, 2020. 33: p. 2958-2969.
34. Schwag, V., et al., Hydra: Pruning adversarially robust neural networks. Advances in Neural Information Processing Systems, 2020. 33: p. 19655-19666.
35. Hendrycks, D., K. Lee, and M. Mazeika. Using pre-training can improve model robustness and uncertainty. in International Conference on Machine Learning. 2019. PMLR.
36. Carmon, Y., et al., Unlabeled data improves adversarial robustness. Advances in Neural Information Processing Systems, 2019. 32.
37. Gowal, S., et al., Uncovering the limits of adversarial training against norm-bounded adversarial examples. arXiv preprint arXiv:2010.03593, 2020.
38. Rebuffi, S.-A., et al., Fixing data augmentation to improve adversarial robustness. arXiv preprint arXiv:2103.01946, 2021.
39. Sridhar, K., et al., Robust Learning via Persistency of Excitation. 2021.
40. Huang, L., C. Zhang, and H. Zhang, Self-adaptive training: beyond empirical risk minimization. Advances in neural information processing systems, 2020. 33: p. 19365-19376.
41. Kim, J. and X. Wang, Sensible adversarial learning. 2019.
42. Zhang, D., et al., You only propagate once: Accelerating adversarial training via maximal principle. arXiv preprint arXiv:1905.00877, 2019.
43. Sitawarin, C., S. Chakraborty, and D. Wagner, Improving adversarial robustness through progressive hardening. 2020.
44. Cui, J., et al., Learnable Boundary Guided Adversarial Training. 2020.
45. Zhang, J., et al. Attacks which do not kill training make adversarial learning stronger. in International Conference on Machine Learning. 2020. PMLR.
46. Pang, T., et al., Boosting Adversarial Training with Hypersphere Embedding. 2020.
47. Rice, L., E. Wong, and Z. Kolter. Overfitting in adversarially robust deep learning. in International Conference on Machine Learning. 2020. PMLR.